Строительные материалы и изделия
Construction Materials and Products

journal homepage: https://bstu-journals.ru

ISSN 2618-7183

DOI: 10.58224/2618-7183-2026-9-5-5

Experimental determination of heat losses through cracks in building walls

Zubarev K.P. * [1, 2, 3], Dobshits V.L. [1], Kazunin V.V. [1], Sapronova Y.A. [2], Fedoseev V.D. [2], Kalinina O.V. [4]

[1] RUDN University, Russia,
[2] National research Moscow State University of Civil Engineering, Russia,
[3] Research Institute of Building Physics of Russian Academy of Architecture and Construction Science, Russia,
[4] Enright Project Construction Limited Liability Company, Russia

Abstract. This study investigates how a repaired crack affects heat losses through a building envelope. An experimental setup was designed and assembled to test wall specimens containing a crack repaired by injection grout. A calculation procedure was developed to determine the specific heat loss through the repaired crack under the conditions of the proposed experimental apparatus. The experimental data were statistically processed using the Shapiro-Wilk test to assess normality. Differences in the specific heat loss before and after crack formation were evaluated with the paired Student's t-test. Statistical significance was accepted at $p < 0.05$. All statistical analyses were carried out in IBM SPSS Statistics. Tests were carried out on foam-concrete, clay brick, and reinforced concrete specimens. Ten specimens were prepared for each material under investigation. During the first stage, intact specimens without cracks were tested. Afterwards, an artificial crack was introduced into each specimen, repaired by injection grouting, and the specimens were tested again under identical conditions. The measured results showed a statistically significant increase in heat loss after crack repair. On average, the specific heat loss increased by 12.1%. The experimental findings were compared with numerical simulations. The temperature field around the repaired crack was calculated by solving the two-dimensional steady-state heat conduction equation. Robin (third-kind) boundary conditions were assigned to the external surfaces exposed to air, Neumann (second-kind) boundary conditions were specified at the truncated boundaries of the computational domain, and fourth-kind boundary conditions were applied at material interfaces. Numerical simulations were performed in ANSYS Workbench 2024. The difference between the numerical predictions and the experimental measurements did not exceed 2.1% for foam concrete, 3.8% for clay brick, and 2.4% for reinforced concrete. The results demonstrate that even after repair, wall cracks noticeably affect the thermal performance of building envelopes. The proposed mathematical model can therefore be used for numerical assessment of heat transfer in walls containing cracks repaired with injection grout.

Keywords: experimental determination, heat conduction problem, cracks, injection grout, thermal conductivity, foam concrete, specific heat loss, model validation

*Corresponding author E-mail: zubarevkirill93@mail.ru

Received May 12, 2026; Received in revised form July 11, 2026; Accepted August 3, 2026

Please cite this article as: Zubarev K.P., Dobshits V.L., Kazunin V.V., Sapronova Y.A., Fedoseev V.D., Kalinina O.V. Experimental determination of heat losses through cracks in building walls. Construction Materials and Products. 2026. 9 (5). 5. DOI: 10.58224/2618-7183-2026-9-5-5

---

1. INTRODUCTION

1.1. Research on Crack Formation in Building Envelopes, Their Detection, and Repair

Crack formation is a common phenomenon that may occur at different stages of a building's service life. As a result, preventing crack initiation, improving crack detection, and developing effective repair technologies remain active areas of research in building science [1-5].

Damage to the thermal envelope can originate from a variety of factors. Among the most common are design deficiencies, construction errors, prolonged operation beyond the intended service life, adverse environmental conditions, anthropogenic influences, and delayed or poor-quality maintenance and repair [6].

Nieto-Julián et al. investigated defects in masonry walls of heritage buildings. Their approach combined terrestrial laser scanning with unmanned aerial vehicle (UAV) surveys, integrating both datasets into a BIM environment. The resulting digital platform stores information on cracks in brick facades together with expert assessments and is intended to support maintenance planning and restoration decision-making for heritage structures [7].

Liu et al. examined crack propagation and failure mechanisms in wall panels used for prefabricated buildings. Their work combined laboratory testing with finite-element simulations performed in ABAQUS 2024. According to their results, increasing the steel thickness from 1.8 to 2.5 mm improved the ultimate load-bearing capacity by 46.15%, while increasing the section height from 80 to 100 mm produced an additional gain of 26.67%. Higher foam concrete strength also increased the cracking load of the panels [8].

Li et al. focused on cracking of plaster layers in external thermal insulation composite systems caused by thermal deformation of insulating materials. Their investigation included numerical simulations in ANSYS followed by full-scale experimental testing. The study concluded that the different thermal responses of insulation materials are mainly governed by variations in the coefficients of linear thermal expansion of the constituent materials. The reported findings provide a basis for further studies on the thermal behaviour of composite insulation systems [9].

Chen et al. explored methods for reducing heat loss while improving the durability of cracked concrete. Fly ash was introduced as an inhibitor to mitigate the alkali–silica reaction. Replacing 20–30% of the cementitious material with fly ash reduced crack development, maintained the mechanical performance of concrete, and lowered the heat flux through the tested specimens by 11.3% [10].

Živanović et al. carried out an experimental investigation into the application of infrared thermography for monitoring the early stages of cement hydration [11].

Reliable detection and continuous monitoring of cracks are essential for assessing the condition of building envelopes. In addition to conventional inspection techniques, recent studies increasingly rely on unmanned aerial vehicles, embedded sensor systems capable of long-term structural monitoring, and artificial intelligence algorithms for automated crack assessment [12].

Ekanayake et al. introduced the CracksGPT visual-language model based on the enhanced MiniGPT-v2 architecture. The network was trained using a dedicated dataset of crack images paired with detailed textual descriptions covering visual characteristics, likely causes, and recommended repair strategies. The proposed system is capable of identifying vertical, horizontal, diagonal, and stepped cracks, determining their probable origin, and suggesting appropriate repair methods. Validation on photographs collected from construction sites demonstrated the practical applicability of the model [13].

Yupanqui et al. proposed a hybrid framework that combines artificial intelligence with finite-element analysis for evaluating masonry walls. The neural network predicts key mechanical properties, including elastic modulus, compressive strength, tensile strength, and fracture energy, directly from crack images. These predicted parameters are subsequently transferred to a finite-element model that simulates the seismic response of the wall. This approach enables machine learning to generate input parameters, while the structural response is computed using a well-established numerical solver [14].

Majumder et al. investigated the use of jute fibre for strengthening masonry structures. Reinforcement with a natural fibre textile-reinforced mortar (TRM) increased the load-bearing capacity of masonry walls by more than 500% and improved thermal insulation by 36%. The strengthened specimens also exhibited higher resistance to crack formation, with the maximum crack width remaining below 7.84 mm [15].

Zheng et al. compiled a database containing 375 images collected from 162 historic buildings. The dataset covers eight categories of surface conditions, including cracks, material damage, missing elements, vandalism, moss, stains, vegetation, and intact areas. It was subsequently used to train an object-detection model based on the YOLOv8 deep-learning architecture for automated defect recognition [16].

Seo et al. developed a convolutional neural network for detecting structural cracks from thermal infrared images. The proposed model achieved an accuracy of 97.72%. The authors reported that most recognition errors were associated with two factors: the presence of multiple objects within a single image and the inherent limitations of the neural network algorithm itself [17].

1.2. Experimental Studies of Heat Transfer through Building Envelope Junctions

Several techniques have been proposed for evaluating the thermal resistance of building envelope systems [18,19]. The conventional approach relies on measuring indoor and outdoor air temperatures together with surface temperatures and heat flux densities recorded on both sides of the building envelope [20].

Experimental investigations differ not only in measurement techniques but also in the design of the testing equipment.

Infrared thermography is one of the most widely used tools for assessing the thermal performance of building envelopes because it enables rapid identification of thermal bridges and other local defects [21-23]. More recently, thermal cameras mounted on unmanned aerial vehicles (UAVs) have been employed to inspect the energy performance of buildings over large areas [24-26]. This technique offers clear visualisation of heat-loss patterns and makes it possible to detect defects across extensive facade surfaces. However, thermal images represent only the thermal state at the moment of acquisition and therefore cannot capture the evolution of heat transfer over time.

Another experimental approach involves embedding temperature sensors directly within the wall structure. Unlike surface measurements, this method allows the internal temperature field to be reconstructed throughout the element [27]. Nevertheless, its practical application is limited because sensors cannot be installed in every type of wall assembly. In addition, the method is intrusive, requiring partial damage to the specimen or structure, which restricts its use primarily to laboratory investigations.

Although numerous studies have addressed thermal performance of building envelopes, relatively little attention has been paid to the influence of injection grout used for crack repair on the resulting heat flow. To address this issue, a dedicated experimental apparatus was developed in the present study for quantifying the specific heat loss associated with repaired cracks in building walls.

The objectives of this study were as follows:

1. to develop an experimental apparatus for measuring the specific heat loss through repaired cracks in building walls;
2. to perform laboratory experiments using the proposed testing system;
3. to compare the experimental measurements with numerical simulation results.

2. METHODS AND MATERIALS

2.1. Experimental Apparatus and Testing Procedure

A dedicated laboratory device was designed to evaluate the specific heat loss through wall cracks repaired with injection grout. The apparatus consists of a U-shaped insulated chamber with thermally protected side walls. One side of the chamber contains an opening into which the tested wall specimen is installed. An electric heating element is mounted on the opposite inner wall to create a controlled temperature gradient across the specimen. Air temperature sensors are positioned both inside and outside the chamber.

A schematic representation of the experimental setup with the installed wall specimen is shown in Fig. 1.

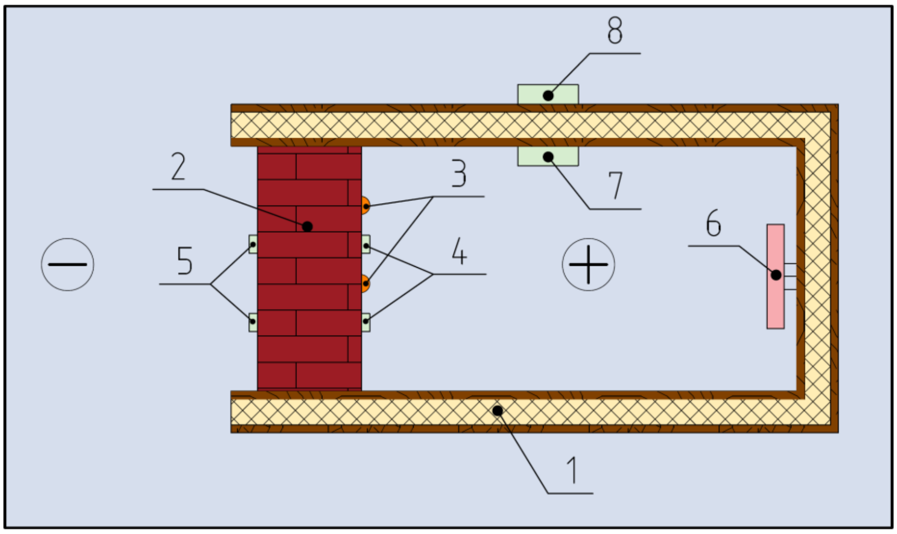

Fig. 1. Schematic layout of the experimental apparatus with the tested wall specimen (1 – insulated chamber; 2 – wall specimen; 3 – heat flux sensors; 4 – internal surface temperature sensors; 5 – external surface temperature sensors; 6 – heating element; 7 – indoor air temperature sensor; 8 – outdoor air temperature sensor).

The experimental programme consisted of two consecutive stages. During the first stage, measurements were carried out using an intact wall specimen without a crack. The same specimen was then provided with an artificial crack, repaired by injection grouting, and tested again under identical boundary conditions.

Heat flux sensors and internal surface temperature sensors were uniformly distributed over the inner face of the specimen. External surface temperature sensors were installed on the opposite side following the same measurement layout.

Photographs of the experimental apparatus with the installed reinforced concrete wall specimen and the placement of temperature and surface heat flux density sensors are presented in Fig. 2.

Each experiment began with activation of the heating element, after which all temperature and heat flux sensors were switched on and continuous data acquisition was initiated.

Throughout the tests, the air temperature inside the chamber was maintained approximately 20 °C higher than the ambient temperature outside the chamber. Steady-state heat transfer was assumed once the temperatures measured on both surfaces of the wall specimen no longer exhibited noticeable variation.

After steady-state conditions had been established, the recorded measurements were used to calculate the specific heat loss through the wall crack repaired with injection grout.

The experimental apparatus for determining the specific heat losses through cracks in building walls filled with injection grout was granted Russian Federation Patent No. 2,866,502 on July 20, 2026.

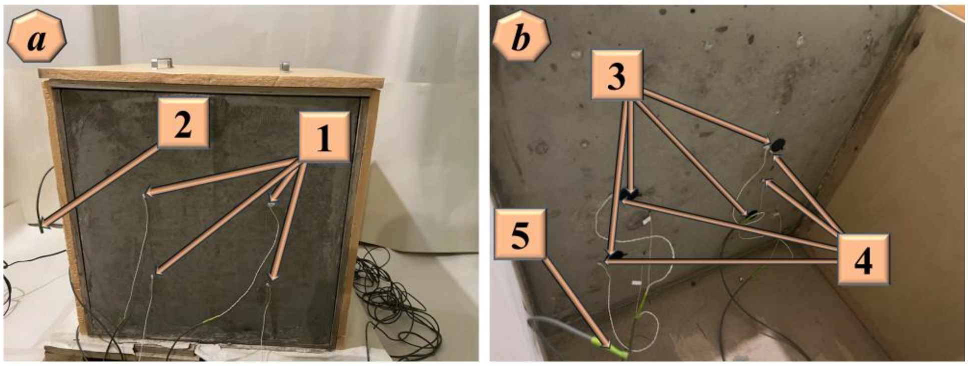

Fig. 2. Experimental apparatus and sensor arrangement on the tested specimen: (a) external view; (b) internal view; 1 – external surface temperature sensors; 2 – outdoor air temperature sensor; 3 – heat flux sensors; 4 – internal surface temperature sensors; 5 – indoor air temperature sensor.

2.2. Derivation of the Equation for Determining Specific Heat Loss Using the Proposed Experimental Apparatus

The experimental programme provided the following measurements:
- temperatures recorded on the external surface of the wall specimen;;
- temperatures recorded on the internal surface of the wall specimen;
- heat flux densities measured on the internal surface of the specimen;
- air temperature outside the experimental apparatus $t_{ext.dev}$;
- air temperature inside the experimental apparatus $t_{in.dev}$;
- surface area of the tested specimen s_{sam}.

The measured data were processed in the following sequence.

First, the average temperature of the external specimen surface was determined $t_{ext.surf.sam}$;

Second, the average temperature of the internal specimen surface was calculated $t_{in.surf.sam}$;

Third, the average heat flux density passing through the internal surface of the specimen was obtained $q_{in.surf.sam}$.

The temperature difference across the specimen $\Delta t_{surf.sam}$ was calculated as:

$$\Delta t_{surf.sam} = t_{in.surf.sam} - t_{ext.surf.sam}. \quad (1)$$

After completion of the first testing stage (intact specimen), the following parameters were determined:

- the temperature difference across the intact wall specimen, $\Delta t_{surf.sam}^{without\ cracks}$;

- the average heat flux density through the intact specimen $q_{surf.sam}^{without\ cracks}$.

After the second testing stage (specimen containing a crack), the following quantities were obtained:

- the temperature difference across the repaired specimen, $\Delta t_{surf.sam}^{with\ cracks}$;

- the average heat flux density through the repaired specimen, $q_{surf.sam}^{with\ cracks}$;

- the total crack length, l_{cracks}.

The specific heat loss associated with the repaired crack was calculated using the formula:

$$\psi_{cracs} = \left(\frac{q_{surf.sam}^{with\ cracks}}{\Delta t_{surf.sam}^{with\ cracks}} - \frac{q_{surf.sam}^{without\ cracks}}{\Delta t_{surf.sam}^{without\ cracks}}\right) \cdot \frac{s_{sam}}{l_{cracks}}. \tag{2}$$

Let us move the term s_{sam} inside the brackets on the right-hand side of the equation:

$$\psi_{cracs} = \left(\frac{q_{surf.sam}^{with\ cracks}}{\Delta t_{surf.sam}^{with\ cracks}} \cdot s_{sam} - \frac{q_{surf.sam}^{without\ cracks}}{\Delta t_{surf.sam}^{without\ cracks}} \cdot s_{sam}\right) \cdot \frac{1}{l_{cracks}}. \tag{3}$$

where ψ_{cracs} – is the specific heat loss attributed to the repaired crack, W/(m·°C).

For convenience, the following quantities are introduced:

$$\chi_{exp}^{with\ cracks} = \frac{q_{surf.sam}^{with\ cracks}}{\Delta t_{surf.sam}^{with\ cracks}} \cdot s_{sam}. \tag{4}$$

where $\chi_{exp}^{with\ cracks}$ denotes the heat-loss coefficient of the wall specimen containing the repaired crack, W/°C.

$$\chi_{exp}^{without\ cracks} = \frac{q_{surf.sam}^{without\ cracks}}{\Delta t_{surf.sam}^{without\ cracks}} \cdot s_{sam}. \tag{5}$$

where $\chi_{exp}^{without\ cracks}$ denotes the heat-loss coefficient of the intact wall specimen, W/°C.

Substituting equations (4) and (5) into equation (3) gives the final expression for calculating the specific heat loss through the repaired crack:

$$\psi_{cracs} = \frac{\chi_{exp}^{with\ cracks} - \chi_{exp}^{without\ cracks}}{l_{cracks}}. \tag{6}$$

2.3. Statistical Analysis of Experimental Data

The distribution of the experimental data was first examined using the Shapiro–Wilk normality test. Differences between the two testing stages were evaluated with the paired Student's t-test. Statistical significance was accepted at a significance level of $p<0.05$.

The paired Student's t-statistic was calculated as:

$$T = \frac{M_d}{\sigma_d / \sqrt{n}}. \tag{7}$$

where T – is the paired Student's *t*-value;

M_d – is the arithmetic mean of the difference between the measured values of specific heat loss;

σ_d – is the standard deviation of these differences;

n – is the number of paired observations.

2.4. Heat Conduction Model for Numerical Simulation of a Wall Specimen Containing a Repaired Crack

The temperature distribution within the wall specimen was simulated by solving the two-dimensional steady-state heat conduction equation:

$$\lambda\left(\frac{\partial^2 t}{\partial x^2} + \frac{\partial^2 t}{\partial y^2} + \frac{\partial^2 t}{\partial z^2}\right) = 0. \tag{8}$$

где λ – теплопроводность, W/(m·°C); t – температура, °C; x, y и z – координаты, m.

where λ – is he thermal conductivity, W/(m·°C); t – is temperature, °C; x, y and z – are the spatial coordinates, m.

The governing equation was solved using the finite element method. Numerical simulations were carried out in ANSYS Workbench 2024.

A computational model reproducing the geometry of the tested wall specimen with a repaired crack was developed for the analysis.

Robin (third-kind) boundary conditions were assigned to all surfaces exposed to air. Neumann (second-kind) boundary conditions were applied at the truncated boundaries of the computational domain, while perfect thermal contact (fourth-kind boundary conditions) was specified at the interfaces between adjacent materials. The numerical model was developed to verify the experimental results by comparing the predicted thermal behaviour with laboratory measurements.

3. RESULTS AND DISCUSSION

3.1. Experimental Evaluation of Specific Heat Loss through a Repaired Crack in Foam Concrete Wall Specimens

The proposed experimental apparatus was manufactured and used for laboratory testing of foam concrete wall specimens.

A total of ten foam concrete specimens were prepared. Each specimen was first tested in its intact condition during the initial stage of the experimental programme. An artificial crack was then introduced, repaired using injection grout, and the specimen was tested again under the same thermal conditions.

Photographs of the tested foam-concrete specimens mounted in the experimental apparatus before and after crack repair are presented in Fig. 3.

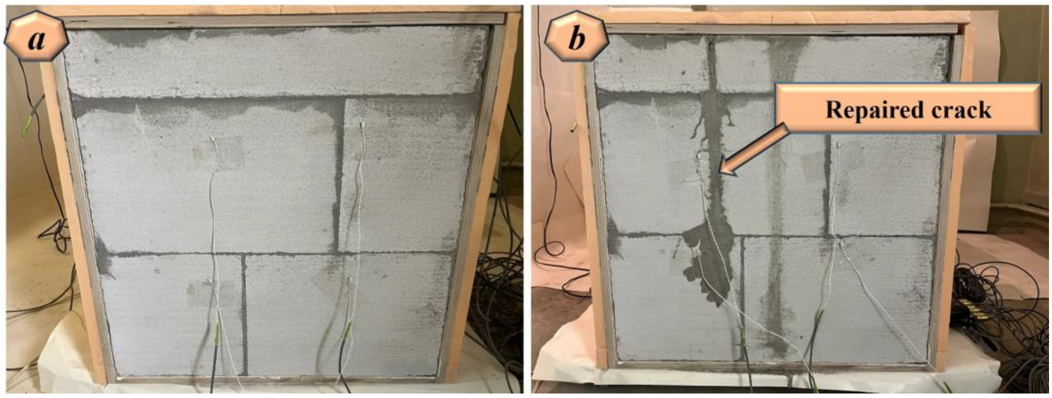

Fig. 3. Foam concrete specimens tested in the experimental apparatus: (a) intact specimen; (b) specimen containing a repaired crack.

The position of the repaired crack in Fig. 3b is indicated by an arrow.

To quantify the thermal influence of the repaired crack, a modified performance indicator was introduced. Instead of using the conventional specific heat loss of the wall specimen, the analysis employed the ratio of the additional heat loss to the crack length, χ / l_{cracks}. This parameter was selected because the reference specimens used during the first testing stage contained no cracks, making the conventional definition of crack-related specific heat loss ψ inapplicable.

The values of χ / l_{cracks} obtained for all tested specimens are presented below.

The experimental programme included ten paired measurements corresponding to the intact and repaired states of each foam concrete specimen. The calculated values of are summarized in Table 1.

Table 1. Specific heat loss per metre of crack for the tested foam-concrete wall specimen, W/(m·°C)/

Test No.	Intact specimen	Specimen with repaired crack
1	0.698	0.795
2	0.699	0.793
3	0.698	0.794
4	0.696	0.793
5	0.697	0.793
6	0.698	0.795
7	0.696	0.794
8	0.695	0.792
9	0.696	0.791
10	0.696	0.793
Average value	0.697±0.0004	0.793±0.0004

The last row of Table 1 reports the average values of the specific heat loss normalized to one metre of crack length.

For the intact specimens, the mean value χ / l_{cracks} was 0.697 W/(m·°C), whereas the repaired specimens yielded an average of 0.793 W/(m·°C). In both cases, the standard error of the mean was 0.0004 W/(m·°C).

The datasets presented in the second and third columns of Table 1 were examined for normality using the Shapiro–Wilk test in IBM SPSS Statistics. Both datasets were found to follow a normal distribution, making parametric statistical analysis appropriate. Since each repaired specimen was tested after measurements had been obtained from the same specimen in its intact condition, the paired Student's *t*-test was selected. The statistical analysis was also performed in IBM SPSS Statistics.

Evaluation using Eq. (7) confirmed that the observed differences between the two testing stages were statistically significant.

The changes in the specific heat loss normalized per metre of crack length before and after crack repair are illustrated in Fig. 4.

The experimental results indicate that the presence of the repaired crack increased the specific heat loss by 12.1%.

The results obtained from the two-stage testing of ten clay brick wall specimens χ / l_{cracks} are summarized in Table 2.

Based on the experimental data, the mean value of χ / l_{cracks} was 1.611 ± 0.0004 W/(m·°C) for the intact specimens and 1.663 ± 0.0003 W/(m·°C) for the specimens containing a repaired crack.

Evaluation using Eq. (7) confirmed that the observed differences between the two testing stages were statistically significant.

The variation in the specific heat loss per metre of crack length before and after crack formation is illustrated in Fig. 6.

As shown in Fig. 6, the specific heat loss increased by 3.1% after the crack had been introduced.

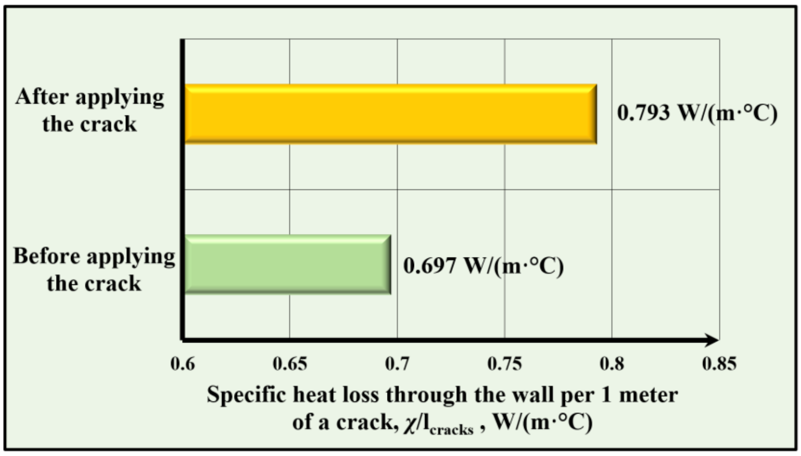

Fig. 4. Bar chart showing the change in the specific heat loss per metre of crack length before and after crack formation for the foam-concrete wall specimens.

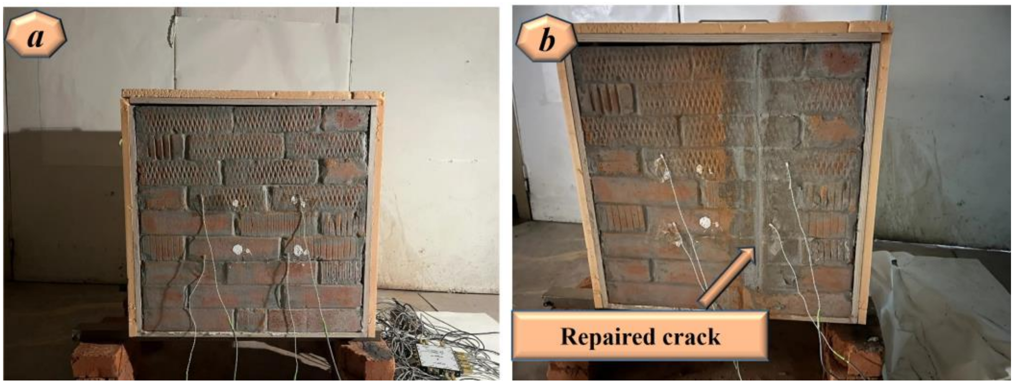

Fig. 5. Photographs of the specimens mounted in the developed test apparatus: (a) intact clay brick wall specimen; (b) clay brick wall specimen with an injection-repaired crack.

Table 2. Specific heat loss per metre of crack length measured for the tested clay brick wall specimens, W/(m·°C).

Test No.	Intact specimen	Specimen with repaired crack
1	1.61	1.664
2	1.612	1.665
3	1.611	1.663
4	1.613	1.662
5	1.611	1.662
6	1.61	1.663
7	1.611	1.665
8	1.613	1.664
9	1.612	1.663
10	1.61	1.663
Average value	1.611±0.0004	1.663±0.0003

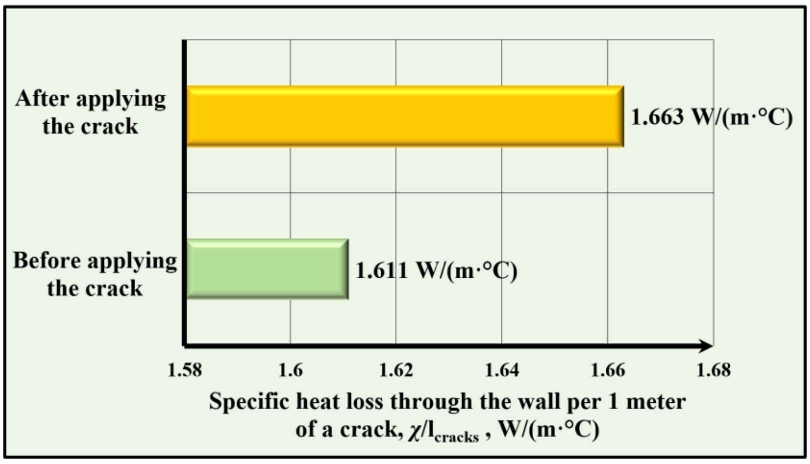

Fig. 6. Bar chart showing the change in the specific heat loss per metre of crack length before and after crack formation for the clay brick wall specimens.

Fig. 7 shows photographs of the reinforced concrete wall specimens mounted in the developed test apparatus, both before crack formation and after repair by injection grouting.

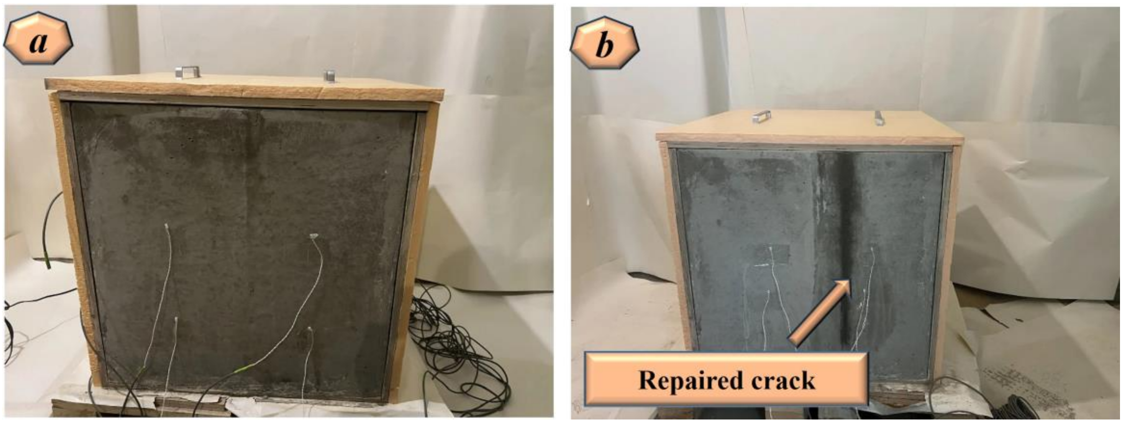

Fig. 7. Photographs of the specimens mounted in the developed test apparatus: (a) intact reinforced concrete wall specimen; (b) reinforced concrete wall specimen with an injection-repaired crack.

The results obtained from the two-stage testing of ten reinforced concrete wall specimens χ / l_{cracks} are summarized in Table 3.

Based on the experimental data, the mean value of χ / l_{cracks} was 3.280 ± 0.0004 W/(m·°C) for the intact specimens and 3.239 ± 0.0004 W/(m·°C) for the specimens containing an injection-repaired crack.

Evaluation using Eq. (7) confirmed that the observed differences between the two testing stages were statistically significant.

The variation in the specific heat loss per metre of crack length before and after crack formation is illustrated in Fig. 8.

As shown in Fig. 8, the specific heat loss decreased by 1.3% after the crack had been introduced.

Table 3. Specific heat loss per metre of crack length measured for the tested reinforced concrete wall specimens, W/(m·°C).

Test No.	Intact specimen	Specimen with repaired crack
1	3.281	3.238
2	3.28	3.237
3	3.278	3.24
4	3.28	3.239
5	3.282	3.238
6	3.279	3.239
7	3.28	3.24
8	3.279	3.239
9	3.281	3.238
10	3.28	3.239
Average value	3.28±0.0004	3.239±0.0003

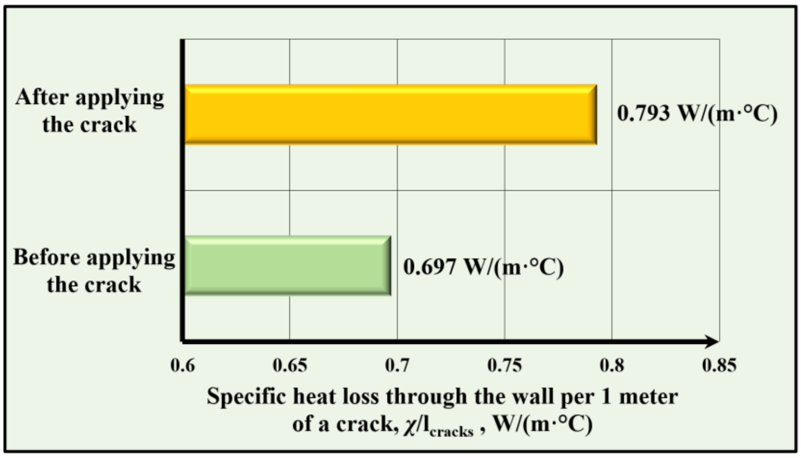

Fig. 8. Bar chart showing the change in the specific heat loss per metre of crack length before and after crack formation for the reinforced concrete wall specimens.

3.2. Comparison of Numerical Predictions with Experimental Measurements

A numerical model of the repaired crack was developed using the measured dimensions of the actual defect. The computational geometry reproduced the dimensions of the wall specimen together with the measured crack width, depth, and height. The resulting temperature distribution obtained from the numerical simulation for the foam-concrete wall specimen is presented in Fig. 9

To evaluate the specific heat loss numerically, calculations were first performed for the intact wall specimen. After obtaining the corresponding temperature field, the linear heat flow rate through the wall $q^L_{\text{without cracks}}$ was determined.

The repaired crack was then introduced into the computational model, and the calculations were repeated under the same thermal boundary conditions to determine the corresponding linear heat flow rate $q^L_{\text{with cracks}}$. In both cases, the temperature difference across the specimen Δt was maintained at 20 °C matching the laboratory experiment.

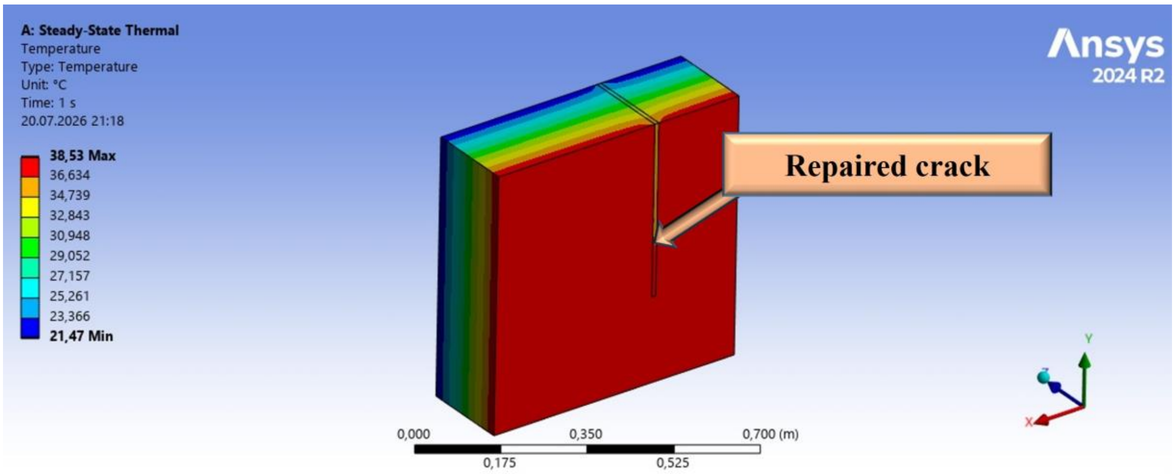

Fig. 9. Temperature field of the foam concrete wall specimen containing a repaired crack.

The specific heat loss associated with the repaired crack was calculated as:

$$\psi = \frac{q^L_{\text{with cracks}} - q^L_{\text{without cracks}}}{\Delta t}. \tag{9}$$

where ψ – is the specific heat loss through the repaired wall crack, W/(m·°C); $q^L_{\text{with cracks}}$ – is the linear heat flow rate through the wall containing the repaired crack, W/m; $q^L_{\text{without cracks}}$ – is the linear heat flow rate through the intact wall, W/m; Δt – is the temperature difference across the specimen °C.

To compare the numerical and experimental results, the values of χ / l_{cracks} obtained by both methods were plotted on the same graph.

A comparison of the specific heat loss normalized per metre of crack length before and after crack repair is shown in Fig. 10.

Figure 10 shows both quantitative and qualitative agreement between the experimental and numerical results. According to both the measurements and the simulation, heat loss through the wall increases when a crack is present.

A direct comparison of the crack-related specific heat loss obtained from numerical modelling and laboratory testing is presented in Fig. 11 and Table 4.

The discrepancy between the numerical prediction and the experimental measurement did not exceed 2.1%, as shown in Table 4 and Fig. 11.

The temperature field calculated for the clay brick wall specimen containing an injection-repaired crack is shown in Fig. 12.

Fig. 13 compares the specific heat loss per metre of crack length in the clay brick masonry wall before crack formation and after crack repair.

Fig. 13 demonstrates good agreement between the experimental measurements and the numerical simulation. Both approaches indicate an increase in heat loss after crack formation and subsequent repair.

A comparison of the crack-related specific heat loss obtained from numerical simulation and laboratory testing for the clay brick wall is presented in Fig. 14 and Table 5.

As indicated by Table 5 and Fig. 14, the discrepancy between the numerical prediction and the experimental measurement for the clay brick wall does not exceed 3.8%.

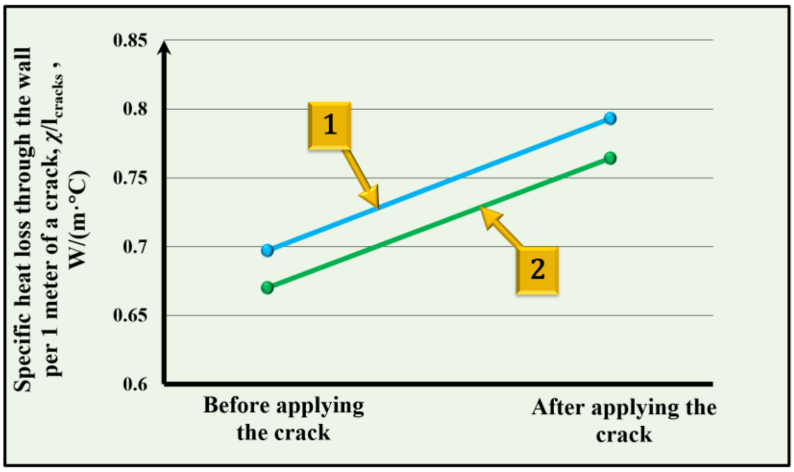

Fig. 10. Comparison of the specific heat loss of foam concrete masonry normalized per metre of crack length before and after crack repair: (1) experimental measurements; (2) numerical simulation.

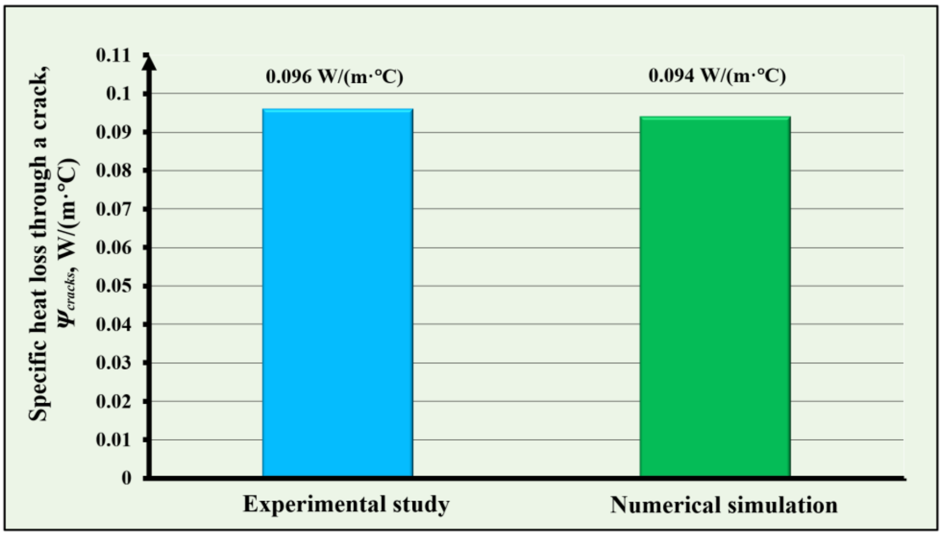

Fig. 11. Comparison of crack-related specific heat loss obtained experimentally and numerically for the foam-concrete wall specimen.

Table 4. Comparison of crack-related specific heat loss obtained from numerical simulation and laboratory testing for the foam-concrete wall specimen.

Specific heat loss ψ_{cracks}, W/(m·°C)		Difference, %
Experimental study	Numerical simulation	
0.096±0.0004	0.094	2.1

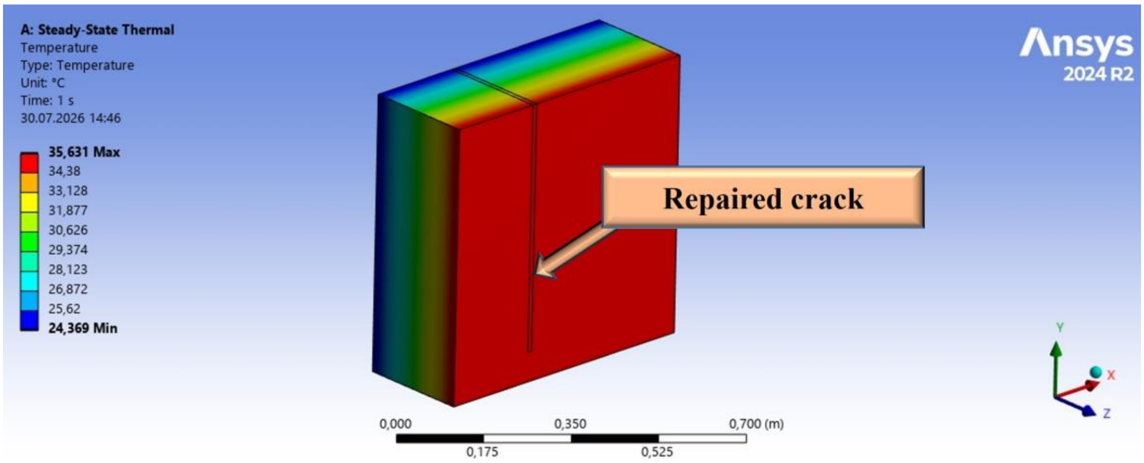

Fig. 12. Temperature field of the clay brick wall specimen containing an injection-repaired crack.

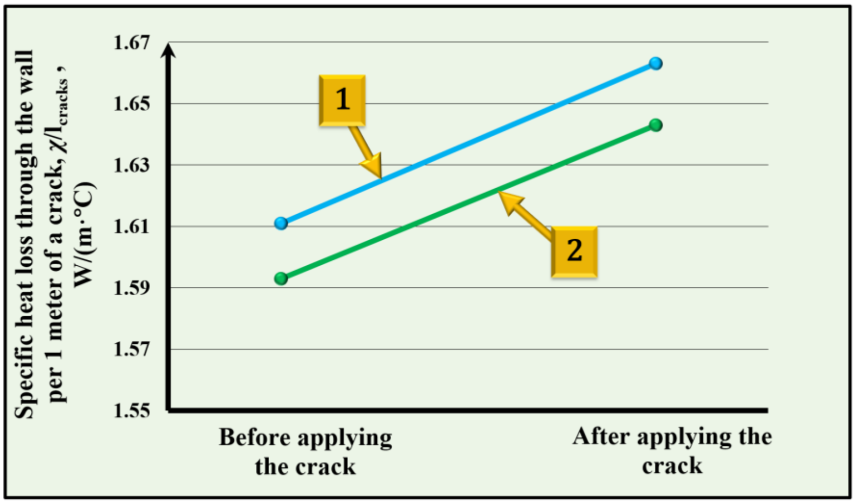

Fig. 13. Comparison of the specific heat loss per metre of crack length for the clay brick masonry wall before crack formation and after crack repair: (1) experimental measurements; (2) numerical simulation.

Table 5. Comparison of crack-related specific heat loss obtained from numerical simulation and laboratory testing for the clay brick masonry wall.

Specific heat loss ψ_{cracks}, W/(m·°C)		Difference, %
Experimental study	Numerical simulation	
0.052±0.0005	0.05	3.8

The temperature field calculated for the reinforced concrete wall specimen containing an injection-repaired crack is shown in Fig. 15.

Fig. 16 compares the specific heat loss per metre of crack length in the reinforced concrete wall before crack formation and after crack repair.

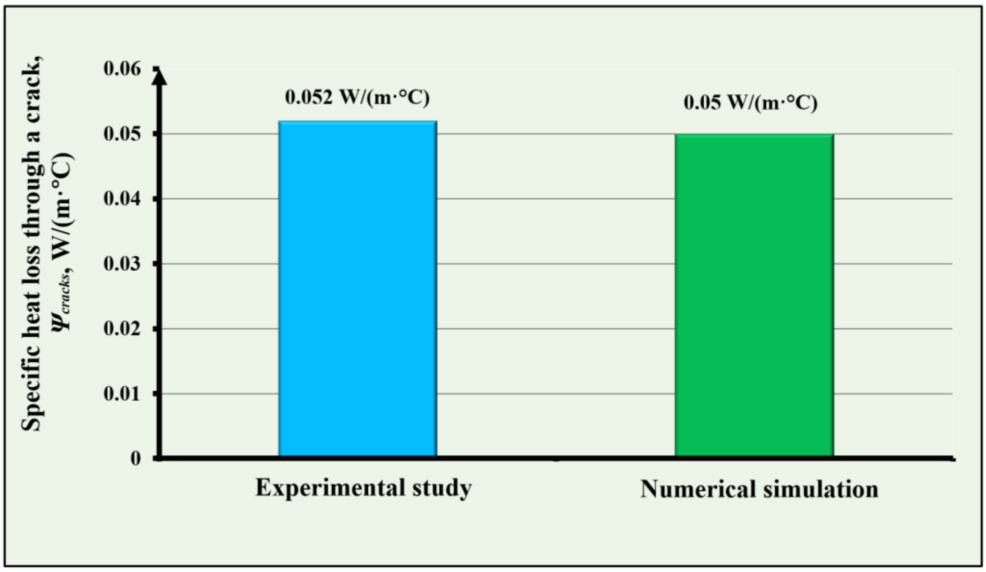

Fig. 14. Comparison of crack-related specific heat loss obtained experimentally and numerically for the clay brick masonry wall.

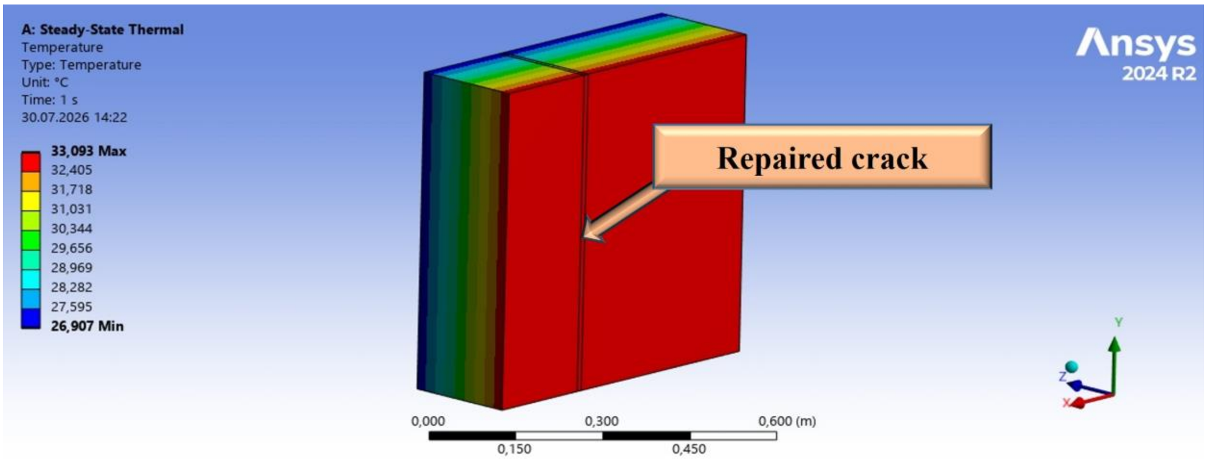

Fig. 15. Temperature field of the reinforced concrete wall specimen containing an injection-repaired crack.

Fig. 16 demonstrates good agreement between the experimental measurements and the numerical simulation. In both cases, the presence of the repaired crack results in a decrease in heat loss through the wall.

A comparison of the crack-related specific heat loss obtained from numerical simulation and laboratory testing for the reinforced concrete wall is presented in Fig. 17 and Table 6.

As indicated by Table 6 and Fig. 17, the discrepancy between the numerical prediction and the experimental measurement for the reinforced concrete wall does not exceed 2.4 %.

Such close agreement confirms that the proposed numerical model adequately reproduces the heat transfer behaviour of repaired wall cracks. The results also demonstrate that repaired cracks continue to affect the thermal performance of building envelopes and that the adopted modelling approach can be used to evaluate this effect with satisfactory accuracy.

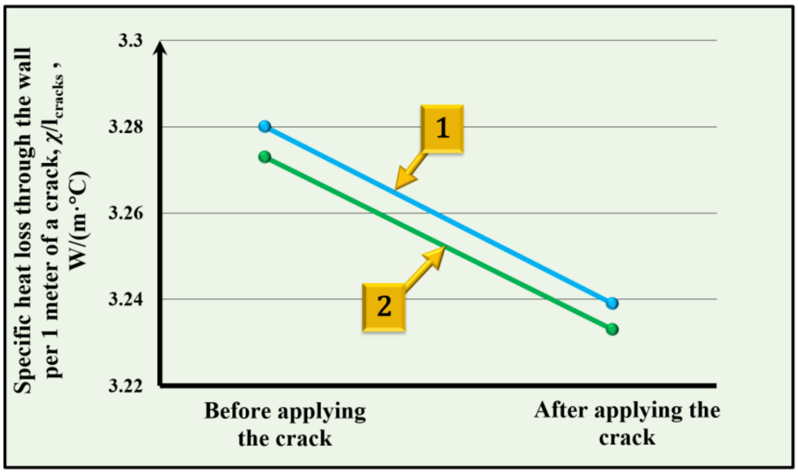

Fig. 16. Comparison of the specific heat loss per metre of crack length for the reinforced concrete wall before crack formation and after crack repair: (1) experimental measurements; (2) numerical simulation.

Table 6. Comparison of crack-related specific heat loss obtained from numerical simulation and laboratory testing for the reinforced concrete wall specimen.

Specific heat loss ψ_{cracks}, W/(m·°C)		Difference, %
Experimental study	Numerical simulation	
-0.041±0.0006	-0.04	2.4

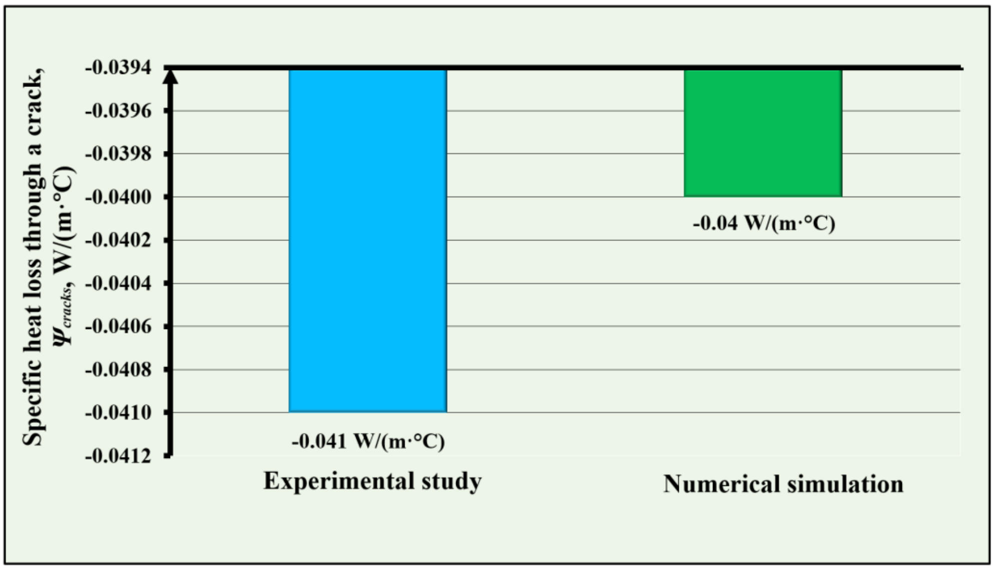

Fig. 17. Comparison of crack-related specific heat loss obtained experimentally and numerically for the reinforced concrete wall specimen.

4. CONCLUSIONS

A laboratory apparatus was developed to quantify the additional heat loss associated with repaired cracks in building walls. The testing procedure consists of two consecutive stages. Measurements are first performed on an intact wall specimen, after which the same specimen is provided with a crack repaired by injection grouting and tested again under identical thermal conditions. An analytical expression was derived for calculating the specific heat loss using the proposed experimental setup.

A three-dimensional steady-state heat conduction model was employed to simulate heat transfer in wall specimens containing repaired cracks. The finite element analysis was carried out in ANSYS Workbench 2024. Robin (third-kind) boundary conditions were assigned to surfaces exposed to air, Neumann (second-kind) conditions were imposed on the truncated boundaries of the computational domain, and thermal contact between adjacent materials was represented by fourth-kind boundary conditions.

Experimental measurements were performed on ten foam concrete wall specimens before crack formation and after crack repair. The numerical simulations reproduced the experimental observations both qualitatively and quantitatively.

The agreement between the computational predictions and the laboratory measurements confirms the validity of the proposed heat-transfer model for building walls containing cracks repaired with injection grout. The developed numerical approach can therefore be used to evaluate the thermal influence of repaired cracks in building envelopes with a high level of confidence.

5. AKNOWLEGMENTS

This publication has been supported by the RUDN University Scientific Projects Grant System, project № 011413-2-000.

REFERENCES

1. Qu S.Y., Pan C.G., Peng B.L., Yue C.H., Fang Z.R., Wen Y.T. Study on the crack resistance of concrete reinforced with flax fiber and multi-walled carbon nano-tubes. Construction and Building Materials. 2025. 488. P. 141884.
2. El Khoury K., Vollum R., Izzuddin B., Forth J. Experimental investigation into cracking in edge restrained concrete walls. Engineering Structures. 2025. 345 (Part B). P. 121536.
3. Li R.G., Cui H.D., Ding L., Ni H.H., Xu S.Q., Wu H.S. Cracking Behavior of Ceramsite Aerated Concrete Block Infill Wall in the Coastal Areas. International Journal of Concrete Structures and Materials. 2025. 19 (1).
4. Tyurina V., Chepurnenko A., Akopyan V. Prediction of Thermal Cracking During Construction of Massive Monolithic Structures. Appl. Sci. 2025. 15 (3). P. 1499.
5. Shalaby Y.M., Badawy M., Ebrahim G.A., Abdelalim A.M. Condition assessment of concrete structures using automated crack detection method for different concrete surface types based on image processing. Discover Civil Engineering. 2024. 1. P. 81.
6. Tazbieva Z.M., Gadaev D.Sh.-B. Causal analysis of defects and assessment of energy efficiency in the examination of the technical condition of buildings and structures. Ekonomika i upravlenie: problemy resheniya. 2026. 2/15 (167). P. 152 – 161.
7. Nieto-Julián E., Robador M.D., Moyano J., Bruno S. Semantic HBIM for Heritage Conservation: A Methodology for Mapping Deterioration and Structural Deformation in Historic Envelopes. Buildings. 2025. 15 (12). P. 1990.
8. Liu X.L., Wang K.P., Zhao Q.B., Luo C.Y. Research on Flexural Performance of Low-Strength Foamed Concrete Cold-Formed Steel Framing Composite Enclosure Wall Panels. Buildings. 2025. 15 (17). P. 3018.
9. Li L.L., Liu J.Y., Li S.Y., Song J.H., Li X., Li J.Y. Thermal Deformation of External Wall Insulation Systems Using EPS, XPS and PU Boards: A Combined Numerical and Experimental Study. Buildings. 2026. 16 (13). P. 2599.

10. Chen L.L., Wei L.L., Zheng J., Zhou J.M. Study on the Inhibition Effect of Fly Ash on Alkali–Silica Reaction and Its Influence on Building Energy Performance. Buildings. 2025. 15 (3). P. 392.
11. Živanović N., Aškrabić M., Savić A., Stević M., Stević Z. Early-Age Cement Paste Temperature Development Monitoring Using Infrared Thermography and Thermo-Sensors. Buildings. 2023. 13 (5). P. 1323.
12. He Y.B., Yuan Z.R., Xia X.H., Yang B., Wu H.T., Fu W., Yao W.X. Local–Global Feature Adaptive Fusion Network for Building Crack Detection. Sensors. 2024. 24 (21). P. 7076.
13. Ekanayake B., Thengane V., Wong J.K.-W., Wilkinson S., Ling S.H. CracksGPT: Exploring the Potential and Limitations of Multimodal AI for Building Crack Analysis. Buildings. 2025. 15 (23). P. 4327.
14. Yupanqui P.R., Orihuela J.L., Delgadillo R.M. Hybrid AI–FEA Framework for Seismic Assessment of Confined Masonry Walls Using Crack Image-Based Material Property Inference. Infrastructures. 2025. 10 (12). P. 323.
15. Majumder A., Valdes M., Frattolillo A., Martinelli E., Stochino F. Natural Fiber TRM for Integrated Upgrading/Retrofitting. Buildings. 2025. 15 (16). P. 2852.
16. Zheng L., Zheng J.Y., Chen Y., Zheng Y.C., Lao W., Chen S.P. Gray Brick Wall Surface Damage Detection of Traditional Chinese Buildings in Macau: Damage Quantification and Thermodynamic Analysis Method via YOLOv8 Technology. Appl. Sci. 2025. 15 (12). P. 6665.
17. Seo H., Raut A.D., Chen C., Zhang C. Multi-Label Classification and Automatic Damage Detection of Masonry Heritage Building through CNN Analysis of Infrared Thermal Imaging. Remote Sens. 2023. 15 (10). P. 2517.
18. Flores Larsen S., Hongn M., Castro N., González S. Comparison of four in-situ methods for the determination of walls thermal resistance in free-running buildings with alternating heat flux in different seasons. Construction and Building Materials. 2019. 224. P. 455 – 473.
19. Leccese F., Salvadori G., Bisegna F. Thermal resilience of buildings: The role of partition walls and slabs in the optimization of the building external envelope. Applied Thermal Engineering. 2024. 257 (9). P. 124084.
20. Bodnar Y., Horon L. Experimental Determination of the Heat Transfer Resistance of the Wall of a Singlestorey Residential Building With a Wooden Frame. Modern technology materials and design in construction. 2025. 38 (1). P. 162 – 166.
21. Tan Y., Huang H., Tang H., Zhang C. Developing thermal point cloud for automated building envelope thermal defects detection. Measurement Science and Technology. 2026. 37 (21). P. 1151 – 1164.
22. Zheng S., Hao F., Lu Y., Jiang T., Yang X. A method for quantitatively evaluating the impact of defects on wall U-value using infrared thermal imaging. Building Simulation. 2025. 18. P. 281 – 293.
23. Mahmoodzadeh M., Gretka V., Mukhopadhyaya P. Challenges and opportunities in quantitative aerial thermography of building envelopes. Journal of Building Engineering. 2023. 69. P. 10621
24. Saei Marand S.A., Mahmoodzadeh M., Mukhopadhyaya P. UAV-Based Infrared Thermography for Qualitative and Quantitative Building Energy Assessment: A Review. Energies. 2026. 19 (7). P. 1776.
25. Videras-Rodríguez M., López-Cabeza V.P., Gómez-Melgar S., Andújar-Márquez J.M. Comparative assessment of quantitative infrared thermography approaches for experimental thermal transmittance determination using UAVs. Building and Environment. 2026. 294. P. 114359.
26. Zhang C., Zou Y., Dimyadi J., Chang R. Thermal-textured BIM generation for building energy audit with UAV image fusion and histogram-based enhancement. Energy and Buildings. 2023. P. 113710.
27. Sassine E., Younsi Z., Cherif Y., Chauchois A., Antczak E. Experimental determination of thermal properties of brick wall for existing construction in the north of France. Journal of Building Engineering. 2017. 14. P. 15 – 23.

INFORMATION ABOUT THE AUTHORS

Zubarev K.P., e-mail: zubarevkirill93@mail.ru, ORCID ID: https://orcid.org/0000-0002-7609-8521, SCOPUS: https://www.scopus.com/authid/detail.uri?authorId=57202815810, Candidate of Engineering Sciences (Ph.D.), RUDN University, Associate Professor of the Department of Construction Technology and Structural Materials, Leading Researcher of the Scientific Center of Engineering and Construction Technologies; National Research Moscow State University of Civil Engineering, Associate Professor of the Department of General and Applied Physics, Associate Professor of the Department of Computer Science and Applied Mathematics, Research Institute of Building Physics of Russian Academy of Architecture and Construction Sciences, Senior Researcher at the Laboratory of Building Thermal Physics

Dobshits V.L., e-mail: 89153383886@mail.ru, ORCID ID: https://orcid.org/0009-0005-9085-6308, RUDN University, PhD Student of the Department of Construction Technology and Structural Materials

Kazunin V.V., e-mail: kvv-vyacheslav@yandex.ru, ORCID ID: https://orcid.org/0009-0000-1005-0069, RUDN University, PhD Student of the Department of Construction Technology and Structural Materials

Sapronova Y.A., e-mail: ho5metown@gmail.com, ORCID ID: https://orcid.org/0009-0007-3032-0995, SCOPUS: https://www.scopus.com/authid/detail.uri?authorId=59235332000, National Research Moscow State University of Civil Engineering, Laboratory Research Assistant of the A.B. Zolotov Research and Education Center of Computer Modelling

Fedoseev V.D., e-mail: fedosseev.vs@gmail.com, ORCID ID: https://orcid.org/0009-0000-9513-8472, SCOPUS: https://www.scopus.com/authid/detail.uri?authorId=59234591700, National Research Moscow State University of Civil Engineering, Laboratory Research Assistant of the A.B. Zolotov Research and Education Center of Computer Modelling

Kalinina O.V., e-mail: Kalinina.kb@yandex.ru, ORCID ID: https://orcid.org/0009-0008-1089-1317, Enright Project Construction Limited Liability Company, Project Manager